NeuroImage: Clinical 12 (2016) 252–261

Contents lists available at ScienceDirect

NeuroImage: Clinical

journal homepage: www.elsevier.com/locate/ynicl

The effective connectivity of the seizure onset zone and ictal perfusion changes in amygdala kindled rhesus monkeys

Evy Cleeren[a,b], Elsie Premereur[a], Cindy Casteels[c,d], Karolien Goffin[c], Peter Janssen[a], Wim Van Paesschen[b,*]

[a] Laboratory for Neuro- and Psychophysiology, KU Leuven, O&N II Herestraat 49 - bus 1021, 3000 Leuven, Belgium
[b] Laboratory for Epilepsy Research, KU Leuven, UZ Herestraat 49 - bus 7003 48, 3000 Leuven, Belgium
[c] Nuclear Medicine & Molecular Imaging, Department of Imaging and Pathology, UZ Herestraat 49 - bus 7003 59, 3000 Leuven, Belgium
[d] Molecular Small Animal Imaging Center (MoSAIC), O&N I Herestraat 49 - bus 505, 3000 Leuven, Belgium

ARTICLE INFO

Article history:
Received 3 February 2016
Received in revised form 4 April 2016
Accepted 31 May 2016
Available online 1 June 2016

Keywords:
Ictal single photon emission computed tomography
Electrical microstimulation
Functional magnetic resonance imaging
Amygdala kindling
Mesial temporal lobe epilepsy

ABSTRACT

Epileptic seizures are network-level phenomena. Hence, epilepsy may be regarded as a circuit-level disorder that cannot be understood outside this context. Better insight into the effective connectivity of the seizure onset zone and the manner in which seizure activity spreads could lead to specifically-tailored therapies for epilepsy.
We applied the electrical amygdala kindling model in two rhesus monkeys until these animals displayed consistent stage IV seizures. At this stage, we investigated the effective connectivity of the amygdala by means of electrical microstimulation during fMRI (EM-fMRI). In addition, we imaged changes in perfusion during a seizure using ictal SPECT perfusion imaging. The spatial overlap between the connectivity network and the ictal perfusion network was assessed both at the regional level, by calculating Dice coefficients using anatomically defined regions of interest, and at the voxel level.
The kindled amygdala was extensively connected to bilateral cortical and subcortical structures, which in many cases were connected multisynaptically to the amygdala. At the regional level, the spatial extents of many of these fMRI activations and deactivations corresponded to the respective increases and decreases in perfusion imaged during a stage IV seizure. At the voxel level, however, some regions showed residual seizure-specific activity (not overlapping with the EM-fMRI activations) or fMRI-specific activation (not overlapping with the ictal SPECT activations), indicating that frequently, only a part of a region anatomically connected to the seizure onset zone participated in seizure propagation.
Thus, EM-fMRI in the amygdala of electrically-kindled monkeys reveals widespread areas that are often connected multisynaptically to the seizure focus. Seizure activity appears to spread, to a large extent, via these connected areas.

1. Introduction

Mesial temporal lobe epilepsy (MTLE) is an electroclinical syndrome whereby seizures originate from the temporal lobe. Seizures can be considered network events involving excessive and re-entrant activation of populations of neurons embedded within brain circuits (Goldberg and Coulter, 2013). In other words, the electrical hyperexcitability associated with seizure activity resonates within the neural structures of the network, which operate together to culminate in the expression of seizures. Furthermore, various imaging modalities have shown widespread cortical and subcortical abnormalities in MTLE, supporting the notion that this type of epilepsy is a network-based disease (Goffin et al., 2011; Laufs et al., 2014; Nelissen et al., 2006; Pittau et al., 2012; Tousseyn et al., 2015; Van Paesschen et al., 2003). Spencer defined a network as a functionally and anatomically connected, bilateral set of cortical and subcortical brain structures or regions in which activity in one part affects activity in all the others (Spencer, 2002). It is possible to observe a dissociation between the structures constituting the neural network underlying a specific patient's epilepsy and the structures involved in seizure propagation: the epileptic network structures are connected (functionally and/or structurally) and are essential to the expression of the seizure, while seizure activity can propagate in a more extensive manner and may involve any neural structure with

Abbreviations: ^{99m}Tc-ECD, 99m-technetium labeled ethyl cysteinate diethylester; EM-fMRI, electrical microstimulation during functional magnetic resonance imaging; MION, monocrystalline iron oxide nanoparticle; MTLE, mesial temporal lobe epilepsy; PSC, percent signal change; SISCOM, subtraction Ictal SPECT co-registered to MRI; SPECT, single photon emission computed tomography; VOI, Volume-Of-Interest.

* Corresponding author at: Laboratory for Epilepsy research, UZ Herestraat 49 box 7003 48, 3000 Leuven, Belgium.
E-mail addresses: evy.cleeren@med.kuleuven.be (E. Cleeren), elsie.premereur@med.kuleuven.be (E. Premereur), cindy.casteels@med.kuleuven.be (C. Casteels), karolien.goffin@uzleuven.be (K. Goffin), peter.janssen@med.kuleuven.be (P. Janssen), wim.vanpaesschen@uzleuven.be (W. Van Paesschen).

http://dx.doi.org/10.1016/j.nicl.2016.05.020

(direct or indirect) anatomical connections to the primary seizure network (Spencer, 2002). Seizure activity can therefore propagate to many more regions than those involved in the epileptic network.

Many studies in human patients have investigated epilepsy networks by measuring the functional connectivity of the presumed seizure focus (Laufs et al., 2014; Pittau et al., 2012; van Mierlo et al., 2014). However, functional connectivity aims to assess connectivity based on statistical dependencies in neuronal activity or activations. Effective connectivity on the other hand, refers to the causal relationships between distinct regions. Effective connectivity can be studied invasively by measuring evoked responses to electrical stimulation applied directly to the brain. Evoked responses can be measured using depth electrodes in distant sites (cortico-cortical evoked potentials) (David et al., 2010) and by electrical microstimulation functional magnetic resonance imaging (EM-fMRI) (Jones et al., 2014; Logothetis et al., 2010; Messinger et al., 2014).

In a previous study, we implemented the electrical amygdala kindling model in rhesus monkeys to study changes in ictal perfusion during kindling epileptogenesis, using ictal SPECT imaging (Cleeren et al., 2015). During amygdala kindling, epileptic seizures were evoked by electrical microstimulation of the amygdala. With daily repetition lasting more than a year, these seizures gradually progressed from interrupting ongoing behavior to secondarily generalized seizures with bilateral clonic movements. We identified a common epileptic network of perfusion changes across the four predefined clinical stages in this model. Furthermore, we found that most longitudinal changes in perfusion originated from this common, initially-activated network. In patients, ictal SPECT imaging is mainly used to detect the seizure onset zone in the presurgical evaluation of intractable epilepsy (Van Paesschen et al., 2007). Due to the low temporal resolution of ictal perfusion SPECT, hyperperfusion patterns generally contain propagation pathways as well.

Because charting anatomically-connected regions of the seizure onset zone is rarely possible in actual patients, we chose to study the effective connectivity of the seizure focus in our kindled monkeys. We therefore investigated the effective connectivity of the kindled amygdala using electrical microstimulation during fMRI (EM-fMRI). We postulate that greater in-depth knowledge of the areas connected to the seizure onset zone may reveal the key nodes of the underlying epileptogenic network which can then be specifically incorporated into tailored therapies such as deep brain stimulation. For this reason we also compared the structures that are connected to the seizure focus (EM-fMRI) in our model with the structures that participate in seizure generation and progression (ictal perfusion SPECT imaging) within the same animals.

2. Materials and methods

2.1. Subjects and amygdala kindling model

All experimental procedures were performed in accordance with EU Directive 2010/63/EU, and were approved by the Ethical Committee at the KU Leuven. Two male rhesus monkeys (*Macaca mulatta*; adult monkey K: 9 kg, juvenile monkey S.: 6 kg) participated in the experiments. A headpost (Crist Instruments, Hagerstown, MD, USA) was implanted on the skull using ceramic screws and dental acrylic. All surgical procedures were performed under isoflurane anesthesia (1%) and strict aseptic conditions. A custom-made bundle of tungsten microelectrodes (7 in monkey S., 3 in monkey K.; 125 μm diameter, impedance at 1 kHz: 130 kΩ; FHC, Bowdoin, ME, USA) was chronically implanted in or near the basomedial nucleus in the right amygdala, based on preoperative structural MR images. Additionally, a low-impedance reference electrode was inserted into the white matter of the frontal lobe. Both animals participated in the amygdala kindling protocol, which has been described previously (Cleeren et al., 2015). In summary, we elicited a seizure by daily electrical stimulation of the amygdala (1 s, 60 Hz, afterdischarge threshold intensity: 1100 μA for monkey K. and 600 μA for monkey S.) while the animal was performing a passive fixation task and was monitored by video-EEG. Electrical pulses were generated with a DS8000 digital stimulator and a DLS100 digital linear stimulus isolator (World Precision Instruments). We electrically stimulated the amygdala in 358 sessions for monkey S. and 344 sessions for monkey K., which encompassed periods of 17 and 16 months for monkeys S. and K., respectively. Both animals progressed from stage I seizures of short duration and minimal behavioral signs to stage IV seizures of longer duration and bilateral motor signs, as described by Wada and colleagues (Wada et al., 1978).

2.2. Electrical microstimulation during fMRI (EM-fMRI)

When the monkeys were fully kindled (stage IV seizures), we applied EM-fMRI to study the effective connectivity of the kindled amygdala. During the EM-fMRI procedure, the monkeys were sedated with a 50/50% mixture of ketamine and medetomidine. Furthermore, they were video monitored throughout the procedure and body temperature was maintained using a heating pad. Functional images were acquired with a 3.0 T full-body scanner (TIM Trio; Siemens) using a gradient-echo T2*-weighted echo-planar imaging (EPI) sequence (40 horizontal slices; TR: 2 s; TE: 16 ms; 1.25 mm^3 isotropic voxels) with a custom-built eight-channel phased-array receive coil, and a saddle-shaped, radial transmit-only coil (Kolster et al., 2009). Before each scanning session, a contrast agent, monocrystalline iron oxide nanoparticle (MION) (Feraheme: AMAG pharmaceuticals; Rienso: Takeda), was injected into the saphenous vein (7-11 mg/kg) (Vanduffel et al., 2001). The scanning protocol consisted of interleaved stimulation and no-stimulation blocks each lasting 40s. During stimulation blocks, the amygdala was stimulated using a square bipolar pulse (pulse width 0.48 ms, frequency 200 Hz, duration 250 ms) every 2500 ms (DS8000 digital stimulator/DLS100 digital linear stimulus isolator, World Precision Instruments). The stimulation intensity was 1000 μA in monkey K. and 800 μA in monkey S. (due to the presence of slight motor signs at 1000 μA). The timing of the EM pulses during the fMRI experiment was computer controlled. We used the same electrodes as in the amygdala kindling protocol. No seizures were evoked during fMRI microstimulation.

Data were analyzed with statistical parametric mapping (SPM5) and BrainMatch software, using a fixed-effect General Linear Model (GLM). Realignment parameters were included as covariates of no interest to remove brain motion artifacts. Spatial preprocessing consisted of realignment and rigid coregistration with the monkey's own anatomical MRI that was warped to the template (McLaren et al., 2009). To compensate for echo-planar distortions in the images, the functional images were warped to the template anatomy using non-rigid matching BrainMatch software (Chef d'Hotel et al., 2002). The functional volumes were then resliced to 1 mm^3 isotropic and smoothed with an isotropic Gaussian kernel (FWHM 1.5 mm). The level of significance was set at $p < 0.05$, corrected for multiple comparisons (family-wise error (FWE)).

Percent signal change (PSC) was calculated in 34 gray matter Volumes-Of-Interest (VOIs) using MarsBaR (v0.41.1). Twenty-eight (14 right, 14 left hemisphere) VOIs were drawn manually using PMOD (v3.1, PMOD Inc., Zurich, Switserland) on the gray matter prior of the template MRI according to the description of Styner and colleagues (Styner et al., 2007): cingulate gyrus, insula, cerebellum, prefrontal lobe, frontal lobe, occipital lobe, limbic temporal lobe, auditory temporal lobe, visual temporal lobe, parietal lobe, hippocampus, amygdala, caudate and putamen. The VOIs of the thalamus, globus pallidus and the entorhinal cortex were delineated based on a standard rhesus monkey brain atlas (Saleem and Logothetis, 2007). Statistical significance of the PSC was tested using MarsBaR (v0.41.1) employing the no-stimulation condition as the baseline. The significance threshold for one-tailed *t*-tests was set at $p = 0.05$, corrected for multiple comparisons (34 *t*-tests calculated; $p = 0.05/34 = 0.0015$). Standard fMRI analysis methods were used, as described in previous studies (Premereur et al.,

2015). Pearson correlation coefficients were calculated between all brain voxels of the fMRI data obtained from monkey K. and monkey S., and between the 2 sessions of both monkeys independently. Statistical significance of these correlations was determined using permutations tests ($p < 0.05$).

2.3. Ictal SPECT perfusion imaging

Animals were scanned once at baseline before the start of kindling and when fully kindled after stable stage IV seizures were observed. During the latter, a seizure was elicited 10 s after intravenous injection of on average 216.4 MBq (range 166.4–244.0 MBq) of 99 m-Technetium labeled ethyl cysteinate diethylester (^{99m}Tc-ECD). Forty minutes postinjection, the monkeys were sedated with a 50/50% mixture of ketamine and medetomidine. SPECT acquisition, reconstruction and analysis were described previously (Cleeren et al., 2015). All analyses were performed in SPM8 (Statistical Parametric Mapping, Wellcome Trust Centre for Neuroimaging, London, UK). Images were analyzed for each monkey separately, using the Subtraction Ictal SPECT co-registered to MRI (SISCOM) technique (O'Brien et al., 1998). In short, baseline and ictal SPECT images were co-registered to the monkeys' anatomical MRI before spatial normalization to a template MRI (McLaren et al., 2009). All extracerebral activity was masked. The baseline image was subtracted from the ictal image after global scaling to the average activity within the brain. This difference image was transformed into a z-score image using the mean and the standard deviation of the differences in all brain voxels. The mean z-score was calculated in the same 34 gray matter VOIs as for the EM-fMRI analysis.

2.4. Comparison of ictal perfusion imaging and EM-fMRI

We compared the ictal perfusion SPECT imaging and EM-fMRI data using a conjunction analysis for each monkey. At a threshold of 1 SD (SPECT) and $p_{uncorrected} < 0.001$ (fMRI), we evaluated which voxels were either activated or deactivated in both modalities (SPECT hyperperfusion and fMRI activation, and SPECT hypoperfusion and fMRI deactivation). To quantify the degree of spatial overlap between these two modalities, we calculated a Dice coefficient for each monkey. A Dice coefficient is an appropriate measure for comparing thresholded images (Dice, 1945). It is defined as twice the number of regions positive for both modalities over the sum of all SPECT-positive and all fMRI-positive regions. Therefore, a Dice coefficient of 1 denotes perfect overlap and of 0 no overlap. We used the VOIs defined for the fMRI and SISCOM analysis to calculate the Dice coefficient: a VOI was labeled as SPECT-positive if it contained at least 200 voxels with suprathreshold SPECT perfusion changes ($SD \geq 1$ or $SD \leq -1$). A similar criterion was used to identify VOIs with significant fMRI activations or deactivations (i.e., at least 200 voxels at $p_{uncorrected} \leq 0.001$). A non-parametric permutation test was applied to determine statistical significance. To that end, a Dice score was calculated between two groups of randomly-selected VOIs, each containing the same number of VOIs as the SPECT-positive and fMRI-positive groups, respectively. This was repeated for 10,000 random selections and the ranking of the monkey's actual Dice score within the distribution of random Dice scores was determined ($p \leq 0.05$, one-tailed distribution). Overlap was evaluated between SPECT hyperperfusions and fMRI activations and between SPECT hypoperfusions and fMRI deactivations.

To define seizure-specific activity, we plotted the voxels showing increases or decreases in perfusion on SPECT (SD 1.5) while excluding voxels showing respective activations or deactivations on fMRI ($p_{corrected} < 0.05$).

3. Results

In our previous study, we investigated how the perfusion network, as measured with ictal SPECT, changed throughout the course of kindling (Cleeren et al., 2015). Therefore, two rhesus monkeys were initially kindled for 17 (monkey S.) and 16 (monkey K.) months, after which we continued with amygdala stimulation to maintain the monkeys in stage IV. A stage IV seizure was characterized by dystonic and clonic movements in all four limbs. In monkey S. these clonic movements always started on the contralateral half of the body and remained asymmetric, whereas in monkey K. symptoms were bilateral from the onset of the seizure, which often made it difficult to lateralize the symptoms based on seizure semiology. The EEG traces recorded during the ictal SPECT experiment in stage IV are shown in fig. 1. Even with prolonged kindling (i.e. more than 1 year after first expressing stage IV seizures), we did not observe spontaneous seizures in our monkeys.

3.1. Effective connectivity of the kindled amygdala

We electrically stimulated the kindled amygdala during two fMRI scan sessions per monkey (15 runs for monkey S. and 20 runs for monkey K.). Fig. 2A and C show the *t*-score maps overlaid on coronal sections for the two monkeys (contrast EM vs No-EM; $p_{corrected} < 0.05$). EM-fMRI of the kindling site in the amygdala evoked extensive fMRI activations and deactivations in the cortical and subcortical structures of both monkeys. In monkey S. (Fig. 3A), significant focal increases in fMRI activity were observed in the VOIs of the ipsilateral thalamus, the contralateral

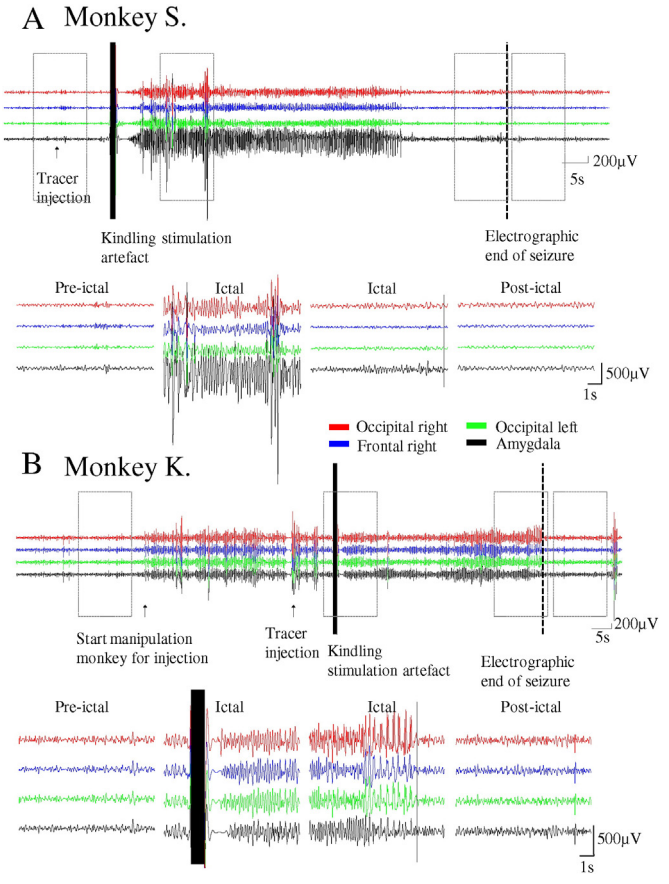

Fig. 1. Pre-ictal, ictal and posticta EEG during ictal SPECT injection. (A) 120 s of depth (right amygdala, black traces) and epidural (occipital right in red, frontal right in blue and occipital left in green traces) EEG of monkey S. during the pre-ictal injection of ^{99m}Tc-ECD. The radiotracer was injected 10 s before eliciting a seizure using the kindling stimulation pulse which generated a 1 s artefact (black rectangle). End of the seizure is denoted with a black dotted line. Four 10 s episodes of EEG, indicated with the gray dotted rectangles are enlarged in the lower panel, (B) 150 s of the EEG signal of monkey K. using the same conventions as in panel A. Note, however, that we observed artefacts before the kindling pulse in this monkey. These artefacts were due to the handling of the monkey during the preparation of the pre-ictal injection of the radiotracer. (For interpretation of the references to color in this figure legend, the reader is referred to the web version of this article.)

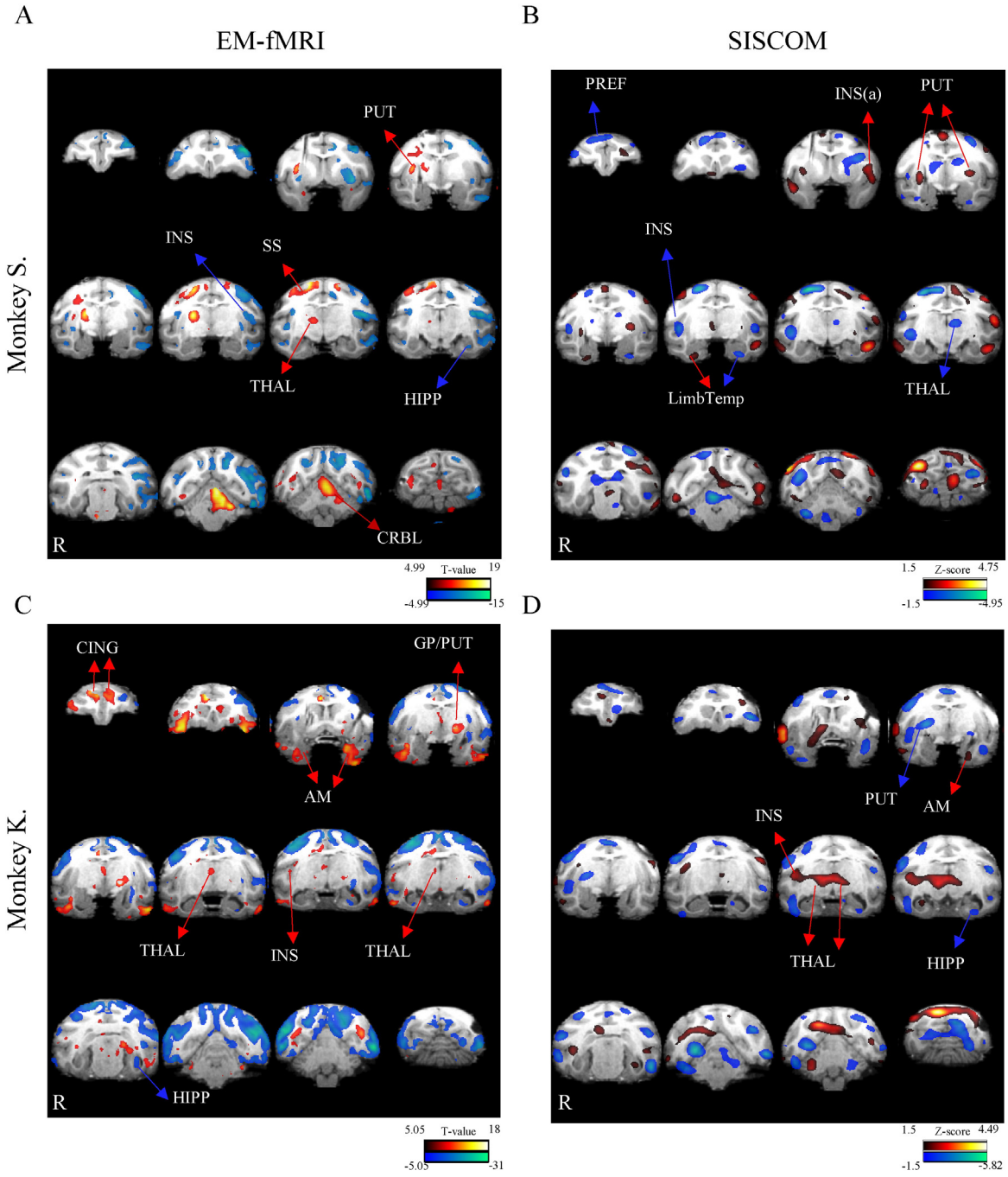

Fig. 2. EM-fMRI and SISCOM results. (A,C) EM-fMRI t-score maps showing activations (red) and deactivations (blue) overlaid on coronal sections of the anatomical MRI of monkey S. (A) and monkey K. (C). EM-fMRI changes were tresholded on $p < 0.05$, FWE-corrected. (B,D) SISCOM z-score maps showing hyperperfusions (red) and hypoperfusions (blue) overlaid on the same coronal sections of both monkeys. Stimulation was performed in the right amygdala. Coronal slices are depicted in radiological convention. AM: amygdala; CING: cingulate gyrus; CRBL: cerebellum; GP: globus pallidus; HIPP: hippocampus; INS: insula; INS(a): anterior insula; LimbTemp: limbic temporal lobe; PREF: prefrontal cortex; PUT: putamen; SS: somatosensory cortex. (For interpretation of the references to color in this figure legend, the reader is referred to the web version of this article.)

globus pallidus and bilaterally in the cerebellum. In addition, smaller activations were observed in the VOIs of the ipsilateral putamen and ipsilateral frontal lobe (somatosensory cortex). The latter activations occupied a smaller part of the respective VOIs, so that the activations in the entire VOI were not significant. In monkey K., however, amygdala EM activated a different network: in contrast to monkey S., the ipsilateral insula, ipsilateral prefrontal cortex, contralateral globus pallidus, and contralateral putamen were activated, in addition to a number of structures that were activated bilaterally: the amygdala, caudate nucleus, thalamus and cingulate cortex (Fig. 3B). Smaller activations were observed bilaterally in the temporal pole, the primary visual cortex and the orbitofrontal cortex. The latter activations comprised only a part of an individual VOI (visual and auditory temporal lobe, occipital lobe, prefrontal and frontal lobe, respectively), so that the entire VOI was not significantly activated.

Amygdala EM also evoked distinct patterns of deactivations in these two monkeys. We observed significant focal decreases in fMRI activity, mainly contralateral to the stimulation site in monkey S., in cortical (auditory and visual temporal, cingulate, prefrontal and parietal cortex) and subcortical (hippocampus, insula and putamen) areas (Fig. 2A and fig. 3A). In monkey K., fMRI deactivations were observed, mainly bilaterally (in frontal, occipital, parietal, and visual temporal cortex), and

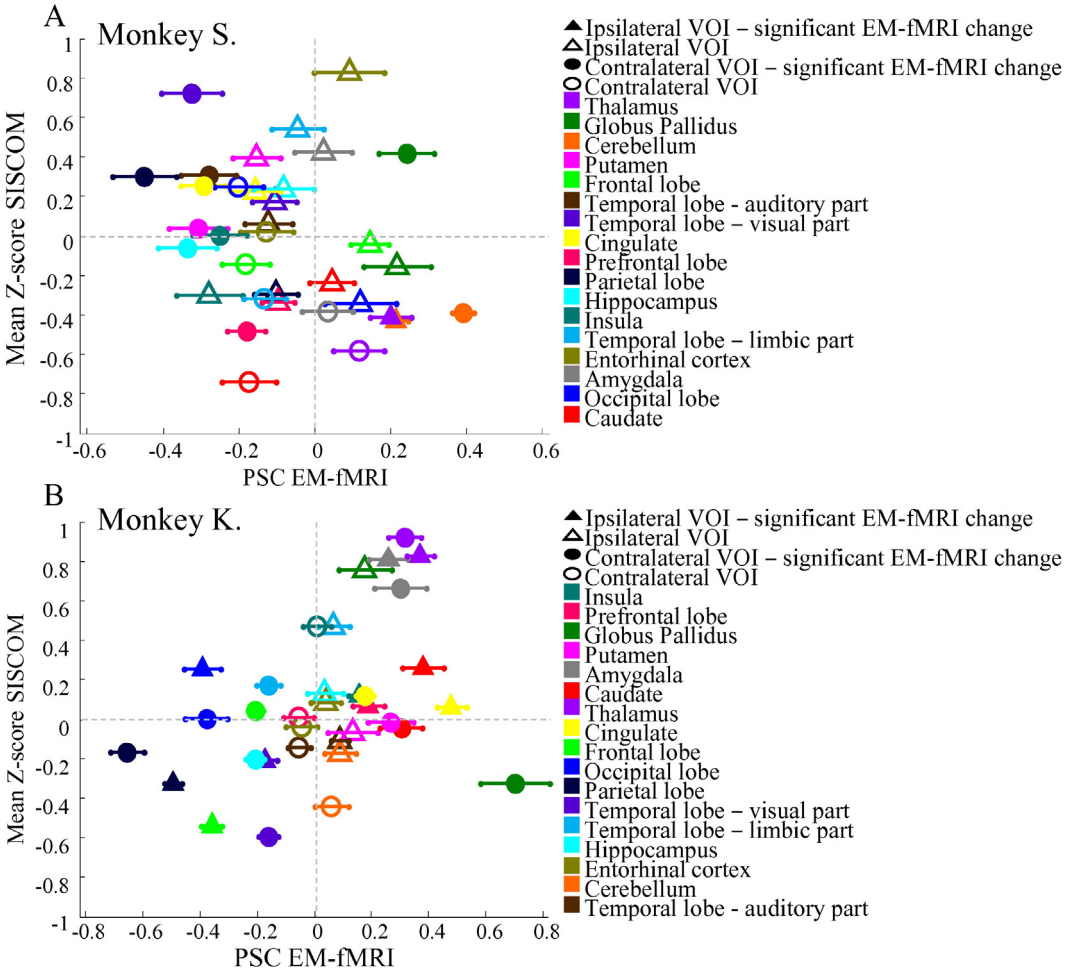

Fig. 3. Percent signal changes and mean z-score per Volume-Of-Interest. Scatterplot plotting the mean z-score in the SISCOM images (y axis) versus the Percent Signal Change (PSC) in the EM-fMRI images (x axis) per Volume-Of-Interest (VOI) for monkey S. (A) and monkey K. (B). Different colors depict the different VOIs, triangles the ipsilateral VOIs, squares the contralateral VOIs. Filled symbols represent the VOIs in which we found a significant activation or deactivation in EM-fMRI images ($p < 0.05$, corrected for multiple comparisons). Horizontal errorbars represents the SEM of the EM-fMRI results. (For interpretation of the references to color in this figure legend, the reader is referred to the web version of this article.)

contralaterally in the limbic temporal lobe including the hippocampus (Fig. 2C and fig. 3B). Note that in the amygdala stimulation site, we observed a significant activation in monkey K., and a non-significant increase in fMRI activity in monkey S., which became apparent at a lower threshold ($p_{uncorrected} < 0.005$) and was attributable to technical limititations.

To quantify the correspondence in EM-evoked fMRI activations and deactivations between the two subjects, we calculated a correlation coefficient between data obtained from each of the two monkeys. We found a weak correlation of 0.32 ($p < 0.001$, permutation test). The disparate patterns of activations evoked by amygdala EM in the two animals were not caused by random variability between sessions, since the correlations between fMRI activations and deactivations measured in sessions 1 and 2 was very high for both subjects (0.67 for monkey S., and 0.74 for monkey K., $p < 0.001$ in the permutation test). We also scanned few runs with stimulation currents of 500 μA, but could not elicit EM-fMRI activations, as reported in a previous study in parietal cortex (Premereur et al., 2015).

Overall, patterns of activation and deactivation evoked by amygdala EM seemed more obviously bilateral in monkey K. compared to monkey S. (Fig. 2A and C), although the actual difference between subjects did not reach significance (ANOVA: PSC as dependent variable, with factors *monkey* and *hemisphere*; p (factor monkey) = 0.07; p (factor hemisphere) = 0.12; p (monkey*hemisphere) = 0.46).

3.2. Brain perfusion changes during a stage IV seizure

During stage IV seizures, we observed widely distributed areas of increased or decreased perfusion compared to the baseline SPECT, in the cortical and subcortical structures in both monkeys. In monkey S. (Fig. 2B and fig. 3A), hyperperfusion was seen in the ipsilateral limbic temporal lobe including the entorhinal cortex, ipsilateral cingulate cortex, contralateral insula, contralateral parietal and occipital lobe and bilaterally in the putamen and auditory and visual portions of the temporal lobe. In contrast, hypoperfusion was more prevalent in the corresponding areas contralateral to the regions of hyperperfusion (which could be either ipsilateral or contralateral to the stimulated hemisphere): in the contralateral limbic temporal lobe including the amygdala and hippocampus, and in the ipsilateral insula, occipital and parietal cortex. Other areas of hypoperfusion comprised the ipsilateral globus pallidus, and bilaterally, the caudate, thalamus, cerebellum and prefrontal and frontal cortex. The SISCOM of monkey K. (Fig. 2D and fig. 3B) showed a different pattern of perfusion change consistent with clinical seizure progression (i.e., greater bilateral involvement) in this animal. We measured hyperperfusion in the ipsilateral caudate, insula and cingulate cortex, the contralateral limbic temporal lobe including the amygdala and the contralateral frontal cortex. Moreover, this monkey also showed hyperperfusion bilaterally in the thalamus, in occipital and prefrontal cortex. Areas of hypoperfusion were found in the ipsilateral frontal

cortex, the contralateral entorhinal cortex, hippocampus and globus pallidus, and bilaterally in the cerebellum, putamen and the parietal, auditory and visual portions of the temporal cortex. Thus, SISCOM analysis demonstrated that stage IV seizures were associated with widespread changes in brain perfusion, which differed between animals and were consistent with seizure propagation.

3.3. Comparison between effective connectivity and ictal perfusion imaging

To assess the overlap between the effective connectivity of the kindled amygdala and the perfusion changes during a seizure initiated in the amygdala, we calculated which voxels showed both an increase (at SD > 1) in perfusion and an fMRI activation ($p_{uncorrected} < 0.001$), as well as voxels which showed a decrease (at SD < −1) in perfusion and an fMRI deactivation ($p_{uncorrected} < 0.001$). Results are shown in Fig. 4, overlaid on the respective MRI. Areas showing hyperperfusion on SPECT and activation on fMRI consisted of the ipsilateral putamen, the ipsilateral sensorimotor cortex, the ipsilateral thalamus, the ipsilateral occipital lobe, the contralateral cerebellum and the Periaqueductal Gray Matter (PAG) in monkey S. In this monkey, we found an overlap between hypoperfusion and fMRI deactivation mainly in the contralateral hemisphere (hippocampus, caudate, putamen and entorhinal, occipital, limbic temporal and frontal cortex) but also bilaterally (insula, parietal, prefrontal and auditory temporal cortex). Note that the ipsilateral putamen contained both fMRI activations and deactivations, and is on average deactivated (Fig. 3A). In monkey K. the conjunction images showed areas of hyperperfusion and fMRI activations in the amygdala, insula and thalamus bilaterally, in the ipsilateral caudate, cingulate, auditory temporal and prefrontal cortex, and in the contralateral limbic temporal lobe. Areas that displayed hypoperfusion and fMRI deactivations comprised the contralateral putamen, entorhinal cortex and the limbic temporal lobe including the hippocampus and areas throughout the cortex bilaterally (frontal, occipital, parietal and the auditory and visual parts of the temporal cortex).

We quantified the degree of overlap between the two imaging modalities using Dice coefficients. The Dice coefficient for hyperperfusion in SPECT (SD > 1) and activation in fMRI ($p_{uncorrected} < 0.001$) equaled 0.60 in monkey S. and 0.83 in monkey K. When we evaluated the overlap between SPECT hypoperfusions (SD < −1) and fMRI deactivations ($p_{uncorrected} < 0.001$), the Dice coefficients were 0.75 in monkey S. and 0.77 in monkey K. All Dice coefficients were statistically significant ($p < 0.002$ or less).

The Dice coefficient estimates the overlap between two imaging modalities at the level of the VOIs, but does not indicate how many individual voxels were activated with the two imaging techniques. Although we measured a significant overlap between the two modalities at the VOI-level, a large proportion of the voxels showing perfusion changes were not activated in the EM-fMRI experiments. Fig. 5 depicts the seizure-specific activities for both monkeys, i.e. the voxels with a perfusion change of more than 1.5 SD excluding the voxels of the EM-fMRI activations/deactivations ($p_{corrected} < 0.05$). In monkey S., seizure-specific hyperperfusion areas comprised 97% of all hyperperfusion voxels (at SD 1.5) and included the contralateral insula, parietal and visual temporal cortex and bilaterally the putamen, occipital and auditory temporal cortex. Seizure-specific hypoperfusion voxels represented 92% of all hypoperfusion voxels (at SD 1.5) and were present in the ipsilateral insula, occipital and parietal lobe and bilaterally in the cerebellum, thalamus, caudate, frontal and prefrontal cortex. In monkey K., the ipsilateral caudate, insula and putamen, the contralateral amygdala, and the thalamus and occipital lobe bilaterally, showed seizure-specific hyperperfusion, which comprised 98% of all hyperperfusion voxels. Seventy-seven percent of all hypoperfusion voxels of monkey K. showed seizure-specific hypoperfusion and included the ipsilateral putamen, ipsilateral frontal cortex, the contralateral cerebellum and contralateral visual temporal lobe. However, if we compare Figs. 4 and 5, we conclude that the majority of regions that showed overlap between perfusion changes and fMRI activations or deactivations and the seizure-specific perfusion changes were actually adjacent to one another (for visualization properties, we combined Figs. 4 and 5 in Supplementary Fig. 1). For example, the ipsilateral putamen of monkey S. showed an overlap between SPECT hyperperfusion and fMRI activation (7% of the hyperperfusion voxels in that VOI), whereas it also contained voxels with seizure-specific hyperperfusion (Fig. 6, top). The same was true of the ipsilateral thalamus in monkey K., where the overlap between hyperperfusion (SD 1.5) and fMRI activation ($p_{corrected} < 0.05$) represented 15% of the hyperperfusion (SD 1.5) in that region (Fig. 6, bottom).

In our previous study (Cleeren et al., 2015), we identified a common network consisting of brain regions that showed altered perfusion in every seizure stage (I-IV). Clinical seizure progression during kindling was associated with an expansion of changes in perfusion originating from the nodes of this common network. We analyzed the extent to which the common network overlapped with the network activated during EM-fMRI using a conjunction analysis (SD > 1 for the SPECT data and $p_{uncorr} < 0.001$ for the EM-fMRI data). Very few brain regions of the common network were also activated during EM-fMRI in stage

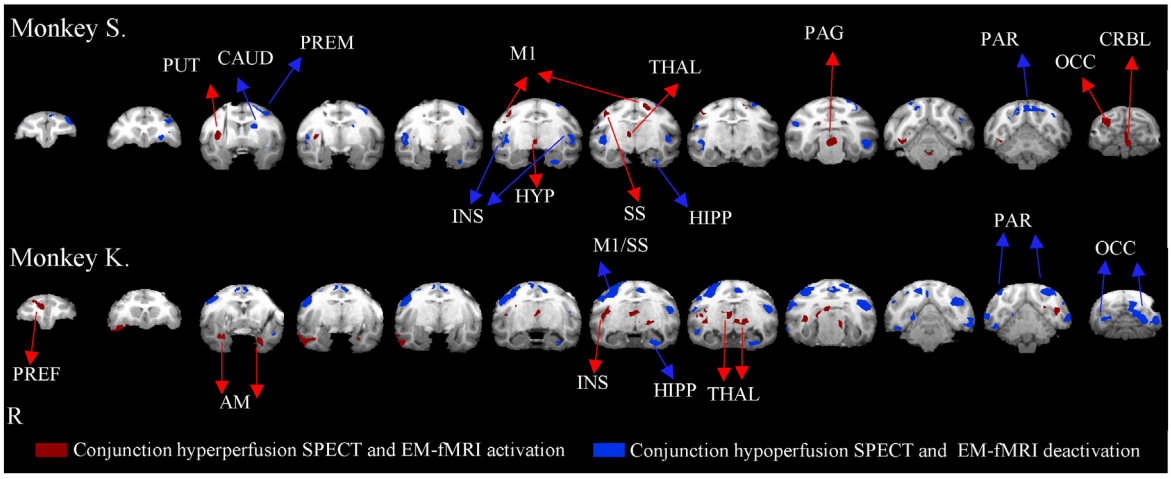

Fig. 4. Conjunction image of SISCOM stage IV (SD 1) and EM-fMRI ($p_{uncorrected} < 0.001$). Coronal slices of both monkeys overlaid with voxels that show a hyperperfusion (SD 1) and an activation on fMRI ($p_{uncorrected} < 0.001$) in red. Voxels showing a hypoperfusion (SD 1) on SPECT and a deactivation on fMRI ($p_{uncorrected} < 0.001$) are overlaid in blue. Only clusters that are at least 400 voxels in size are depicted. AM: amygdala; CAUD: caudate; CRBL: cerebellum; HIPP: hippocampus; HYP: hypothalamus; INS: insula; M1: primary motor cortex; PAG: periaqueductal gray; PAR: parietal cortex; PREF: prefrontal cortex; PREM: premotor cortex; PUT: putamen; SS: somatosensory cortex; THAL: thalamus; OCC: occipital cortex. (For interpretation of the references to color in this figure legend, the reader is referred to the web version of this article.)

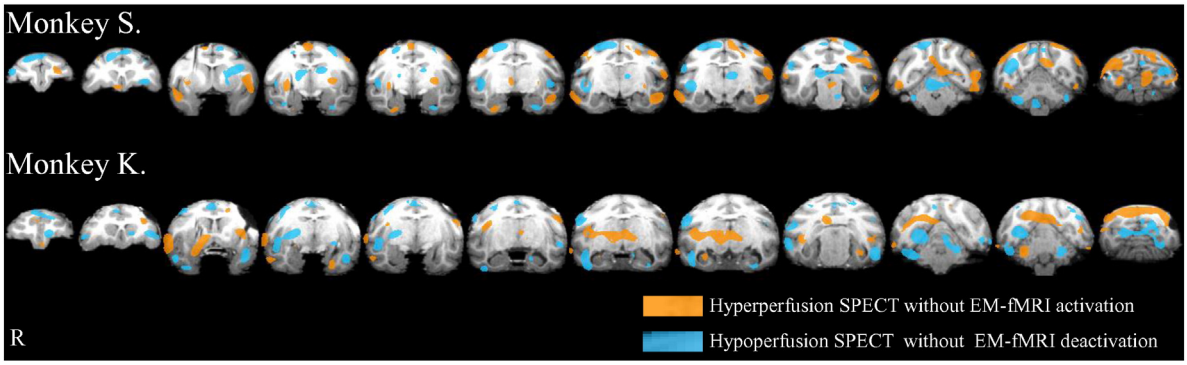

Fig. 5. Seizure specific activity. Hyperperfusion areas during a stage IV seizure (SD 1.5), excluding the voxels that were activated during EM-fMRI ($p_{corrected} < 0.05$) overlaid in orange. Hypoperfusion areas (SD 1.5) excluding the voxels that were deactivated during EM-fMRI (pcorrected < 0.05) are shown in light blue. (For interpretation of the references to color in this figure legend, the reader is referred to the web version of this article.)

IV (Fig. 7, red and blue): in monkey S. the ipsilateral putamen and the hypothalamus, and in monkey K. the ipsilateral prefrontal cortex, amygdala, insula and thalamus. Conversely, the network activated during EM-fMRI excluding the common network was very extensive (Fig. 7, orange and light blue). Thus, the network of brain regions effectively connected to the stimulation site in the amygdala in stage IV overlapped only partially with the common seizure network.

4. Discussion

Our study is the first systematic comparison between the effective connectivity of the seizure onset zone in kindled animals (as measured with EM-fMRI) and seizure-induced perfusion changes (assessed with ictal SPECT imaging). We observed widespread fMRI activations and deactivations evoked by electrical microstimulation in the amygdala, which partially overlapped with the perfusion changes measured with ictal SPECT. These results demonstrate that, subsequent to prolonged kindling lasting more than a year, amygdala microstimulation can activate a very large number of brain regions, some of which are not anatomically connected with the amygdala.

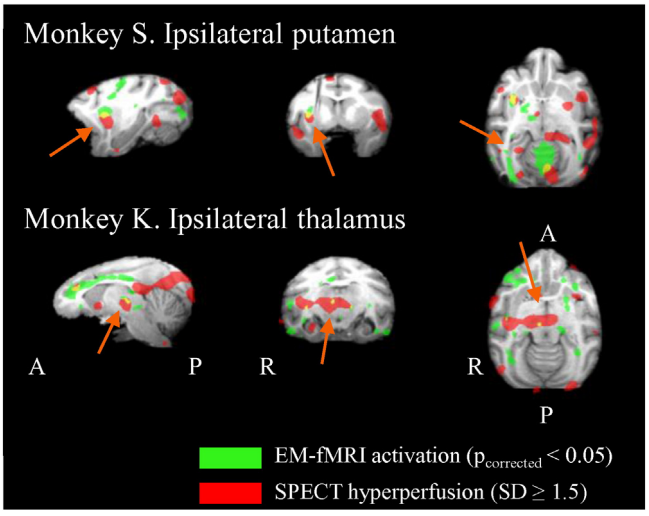

Fig. 6. Examples of the overlap between EM-fMRI activations and SPECT hyperperfusions. (Top) In monkey S. the ipsilateral putamen (orange arrows) is activated in the EM-fMRI experiment (green) and exhibits a hyperperfusion on stage IV SPECT imaging (red). The overlap (yellow) comprises only a part of both activations, indicating that both the seizure specific activity (SPECT hyperperfusion but no EM-fMRI activation) and the EM-fMRI specific activity (EM-fMRI activation but no SPECT hyperperfusion) are adjacent to the overlap. (Bottom) The same holds true in the ipsilateral thalamus (orange arrows) in monkey K. A: anterior; P: posterior; R: right. (For interpretation of the references to color in this figure legend, the reader is referred to the web version of this article.)

EM-fMRI is a relatively new technique that can yield novel information about the effective (i.e. causally related to) connectivity of brain regions in monkeys. Previous EM-fMRI studies have been primarily conducted in cortical areas in frontal, temporal, parietal and occipital cortex, and the Lateral Geniculate Nucleus (Ekstrom et al., 2008; Logothetis et al., 2010; Moeller et al., 2008; Premereur et al., 2015; Tolias et al., 2005). Although interpretation problems related to the ortho- or antidromic nature of the observed effects still remain, these studies have generally demonstrated that EM-fMRI can provide a very detailed map of the anatomical connectivity of the stimulation site (which is much smaller than a cortical area). For example, Premereur and colleagues stimulated various cortical sites in the intraparietal sulcus during fMRI (Premereur et al., 2015), and observed a pattern of connectivity that almost exactly matched the known monosynaptic connectivity of this brain region (Borra et al., 2008). In our study, however, we observed EM-induced activations in brain regions known to be anatomically connected to the basomedial nucleus of the amygdala (e.g., caudate nucleus, putamen, insula), but also in brain regions that are not directly connected to the amygdala, such as the cerebellum, globus pallidus and contralateral thalamus. Hence, prolonged kindling may have changed the connectivity of the stimulation site with remote areas, such that the EM-induced activation propagated more strongly in a multisynaptic manner, which may explain why seizure severity increased and seizures secondarily generalized during the process of kindling. It should be noted that this interpretation of our results should be considered tentative since we did not acquire EM-fMRI data before kindling. Messinger and colleagues applied EM-fMRI in naïve monkeys and found similar widespread fMRI activations, depending on which amygdaloid nucleus was stimulated (Messinger et al., 2014). Besides EM-induced activations we found extensive and bilateral fMRI deactivations elicited by amygdala microstimulation. The physiological meaning of these deactivations is not clear but in line with previous studies applying EM during fMRI in patients with epilepsy and Parkinson's disease (Jones et al., 2014; Stefurak et al., 2003) and in naive and kindled rats (Dunn et al., 2009).

In our previous study (Cleeren et al., 2015), we investigated how the ictal perfusion network evolved through the different stages of amygdala kindling in our rhesus monkeys. During stage IV, the monkeys experienced bilateral motor symptoms (i.e. secondarily generalized seizures) during the seizures evoked by electrical stimulation of the amygdala. Ictal perfusion imaging showed a widespread network of increases and decreases in perfusion in both hemispheres. Because little is known about the relationship between ictal perfusion changes and the connectivity of the seizure onset zone, we here compared the perfusion changes during a stage IV seizure, as measured with ictal perfusion SPECT imaging, with the effective connectivity of the amygdala in the same seizure stage by means of EM-fMRI. Comparing SPECT and EM-fMRI at the voxel level might be difficult, because the underlying

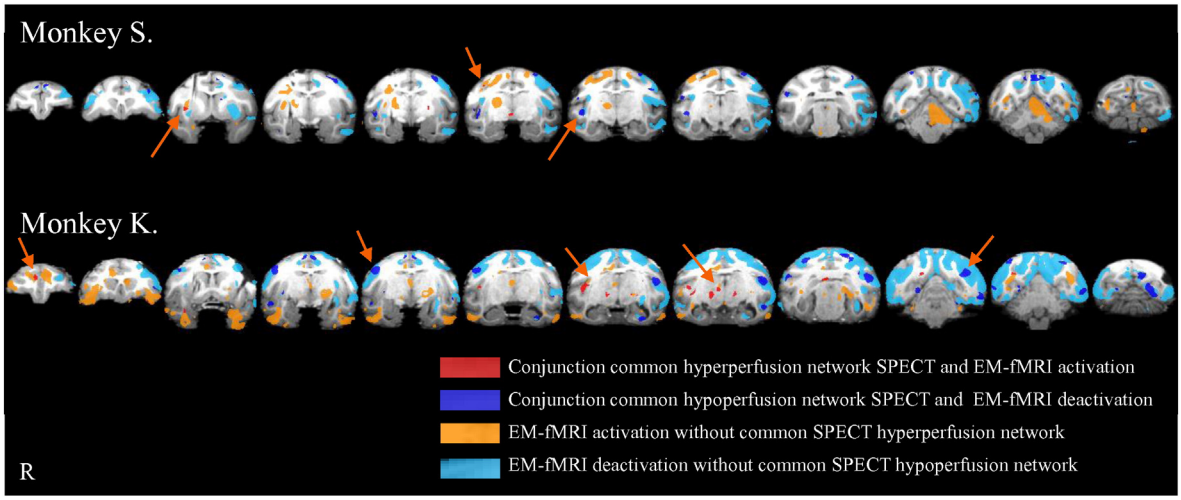

Fig. 7. Overlap between the common SPECT network and EM-fMRI during stage IV of amygdala kindling. Overlap between the common SPECT network (at SD 1) and the EM-fMRI changes ($p_{uncorrected} < 0.001$). The common SPECT network is a network of perfusion changes that were common to the four different seizure stages during amygdala kindling in a rhesus monkey. Overlap was considered between hyperperfusion and EM-fMRI activation (red) and hypoperfusion and EM-fMRI deactivation (blue). Additionally, this figure depicts the EM-fMRI changes ($p_{corrected} < 0.05$) excluding the perfusion changes of the common SPECT network in orange (EM-fMRI activations excluding the common hyperperfusion voxels) and light blue (EM-fMRI deactivations excluding the common hypoperfusion voxels). In many areas (orange arrows), the conjunction image is adjacent to the EM-fMRI activations/deactivations, showing that the common perfusion network is part of the connected network. (For interpretation of the references to color in this figure legend, the reader is referred to the web version of this article.)

physical principles (gamma rays vs paramagnetic changes due to blood volume changes measured with MION, different spatial and temporal resolutions…) differed between the two techniques. Therefore, we chose to determine the spatial overlap of the thresholded images at a regional level using Dice coefficients. We found that the ictal SPECT perfusion changes partially overlapped with the fMRI activations induced by electrical stimulation, for example in the ipsilateral putamen, ipsilateral hypothalamus and the contralateral cerebellum in monkey S. and in the ipsilateral anterior cingulate, ipsilateral posterior insula and ipsilateral thalamus in monkey K.

However, if we focus on the SPECT perfusion changes on the voxel level outside the overlap between the two modalities, we find that the majority of voxels were seizure-specific (i.e. are only suprathreshold in SPECT and not in fMRI) (Fig. 5). These perfusion changes could indicate propagation of epileptic activity to brain regions not directly connected to the amygdala. Indeed, most regions of seizure-specific perfusion changes were located adjacent to the EM-induced fMRI activations and deactivations. Very few regions, for example, the ipsilateral supplementary motor area in monkey S. and the ipsilateral ventral pallidum in monkey K., showed increased perfusion during the seizure, but were not connected to the amygdala based on the fMRI experiment. On the other hand, we also found some regions that did not show changes in perfusions, but were connected to the amygdala (for example the ipsilateral pallidum in monkey S. and the ipsilateral temporal pole and entorhinal cortex in monkey K.). The functional relevance of these dissociations between SPECT and EM-fMRI is not clear at present. One explanation could be that these areas serve as a defense mechanism to prevent seizure activity from spreading. Another possibility is that these areas do participate in the seizure, but only in some later phase of the seizure. Due to the kinetics of the ^{99m}Tc-ECD radiotracer and the preictal injection (which was necessary due to the limb movements during the seizure), we captured only the first 20 s of the seizure (Walovitch et al., 1989). A previous study in kindled rats, however, has shown that the autoradiographically measured perfusion changes are similar when tracer injection occurred preictally or at the time of seizure onset (Chassagnon et al., 2005).

Our previous study indicated that the epileptogenic network is activated early during kindling epileptogenesis, which allowed us to define a common network consisting of areas displaying an increase or decrease in every seizure stage of the amygdala kindling model (Cleeren et al., 2015). Because this common network represents the earliest and most consistent changes, we investigated the overlap between the EM-fMRI changes and this common network (Fig. 7). We concluded that most nodes of the common network are part of the EM-fMRI evoked network. As the EM-fMRI network is more widespread than the common network, the EM-fMRI network must contain propagation pathways as well. Note that, although we could not obtain EEG during fMRI, we did not evoke a seizure during EM-fMRI. First, the charge applied during EM-fMRI was 31 to 46 times less than the charge necessary to evoke a seizure (as during kindling). Second, video monitoring and realignment parameters showed no movement and, third, analysis of the no-stimulation blocks also showed no seizure activity.

Since the concept of epilepsy as a network-based disease is gaining acceptance, knowledge of large-scale brain networks has become more relevant (Spencer, 2002; Tousseyn et al., 2015; Yaffe et al., 2015). In this network theory, it might be possible to interfere with seizure propagation by interrupting the network in one of its nodes, even if the seizure onset zone is unknown or contains eloquent cortex and cannot be resected. A prerequisite to use this network approach for therapeutic purposes is that the network nodes are easily and reliably delimited, because they often cross anatomical borders or contain only a part of an anatomical structure. Ictal SPECT imaging is routinely used in patients with epilepsy to identify the origin of seizure activity. SPECT imaging has, however, a low spatial resolution and generally contains both the seizure onset zone and spread (Dupont et al., 2006). EM-fMRI has a better spatial resolution than SPECT, while still sampling the whole brain (in contrast with the limited sampling of intracranial recordings). The effective connectivity measures of the seizure onset zone gives invaluable information about the network nodes that are connected to the seizure onset zone, which could then be targeted for further diagnostic or therapeutic evaluation. EM-fMRI has the additional advantage that all the nodes of the network can be studied systematically in contrast to anatomical tracer studies. However, this systematic study can only be done in an animal model. Several potential hazards, such as heating of the tissue or inducing high currents, are a potential concern for EM-fMRI in patients (Georgi et al., 2004). However, few reports of EM-fMRI in patients are available (Jones et al., 2014; Stefurak et al., 2003). In a small group of patients with epilepsy, Jones and colleagues investigated the potential use of low frequency (20 Hz) EM-fMRI under general anesthesia for identifying the epileptogenic zone (Jones et al., 2014). After resection, the epileptogenic tissue that surrounded the stimulating electrode contacts showed no thermal

damage. An ongoing study evaluated cortico-cortical evoked potentials in patients with implanted depth electrodes. Similar to our study, SISCOM perfusion changes occurred mainly in brain regions showing a microstimulation-induced evoked potential, indicating that perfusion changes propagate through long-range connections (Tousseyn et al., personal communication).

The electrical amygdala kindling model is a valid model to study changes due to temporal lobe seizures and epileptogenesis. An important feature of this model is the progressive nature of the seizure severity. There is an evolution from focal seizures to complex focal seizures with secondarily generalization with daily stimulations (Sutula and Ockuly, 2006). In humans, the existence of kindling and the 'seizures begets seizures' theorem is still debated (Gowers, 1881). Mesial temporal lobe epilepsy has many features of a progressive disease, as evidenced by silent intervals, often after an initial precipitating injury, and the progressive evolution of seizure semiology (French et al., 1993; Mathern et al., 1995).

EM-fMRI of the kindled amygdala generated well-localized but extensive and bilateral fMRI changes throughout cortical and subcortical structures in both subjects. Since we studied only two monkeys, group data could not be calculated. Consistent with our previous work, effective connectivity patterns also differed between the two animals, most likely caused by small differences in the anatomical locations of the electrodes. In patients with epilepsy, the underlying epileptogenic networks can also be different, even within the same epilepsy syndrome (Ho et al., 1996). Mapping the network of both seizure-induced perfusion changes and the connectivity of the seizure onset zone in our monkey model can provide more information about how the seizure activity spreads through anatomically connected areas. However, since EM-fMRI generates diffuse activations, this technique should be combined with other modalities for determining the epileptogenic network in order to provide a more informed basis for tailoring new therapies, such as the identification of target regions for resective surgery or Deep Brain Stimulation for intractable epilepsy.

Supplementary data to this article can be found online at http://dx.doi.org/10.1016/j.nicl.2016.05.020.

Acknowledgements

This work was supported by the Fund for Scientific Research Flanders (G.0745.09) and the Programma Financiering (PFV/10/008). We thank Ann Van Santvoort, Kwinten Porters, Peter Vermaelen, Johan Nuyts, Christophe Ulens, Inez Puttemans, Piet Kayenbergh, Gerrit Meulemans, Jan Lenaerts, Stijn Verstraeten, Wouter Depuydt, Marc De Paep, Astrid Hermans and Sara De Pril, for technical and administrative assistance, and Steve Raiguel for comments on a previous version of this manuscript.

References

Borra, E., Belmalih, A., Calzavara, R., Gerbella, M., Murata, A., Rozzi, S., Luppino, G., 2008. Cortical connections of the macaque anterior intraparietal (AIP) area. Cereb. Cortex 18, 1094–1111.

Chassagnon, S., de Vasconcelos, A.P., Ferrandon, A., Koning, E., Marescaux, C., Nehlig, A., 2005. Time course and mapping of cerebral perfusion during amygdala secondarily generalized seizures. Epilepsia 46, 1178–1187.

Chef d'Hotel, C., Hemosillo, G., Faugeras, O., 2002. Flows of diffeomorphisms for multimodal image registration. Proc. IEEE Int. Symp. Biomed Imaging 7, 753–756.

Cleeren, E., Casteels, C., Goffin, K., Janssen, P., Van Paesschen, W., 2015. Ictal perfusion changes associated with seizure progression in the amygdala kindling model in the rhesus monkey. Epilepsia.

David, O., Bastin, J., Chabardes, S., Minotti, L., Kahane, P., 2010. Studying network mechanisms using intracranial stimulation in epileptic patients. Front. Syst. Neurosci. 4, 148.

Dice, L.R., 1945. Measures of the amount of ecologic association between species. Ecology 26, 297–302.

Dunn, J.F., Tuor, U.I., Kmech, J., Young, N.A., Henderson, A.K., Jackson, J.C., Valentine, P.A., Teskey, G.C., 2009. Functional brain mapping at 9.4T using a new MRI-compatible electrode chronically implanted in rats. Magn. Reson. Med. 61, 222–228.

Dupont, P., Van, P.W., Palmini, A., Ambayi, R., Van, L.J., Goffin, J., Weckhuysen, S., Sunaert, S., Thomas, B., Demaerel, P., Sciot, R., Becker, A.J., Vanbilloen, H., Mortelmans, L., Van, L.K., 2006. Ictal perfusion patterns associated with single MRI-visible focal dysplastic lesions: implications for the noninvasive delineation of the epileptogenic zone. Epilepsia 47, 1550–1557.

Ekstrom, L.B., Roelfsema, P.R., Arsenault, J.T., Bonmassar, G., Vanduffel, W., 2008. Bottom-up dependent gating of frontal signals in early visual cortex. Science 321, 414–417.

French, J.A., Williamson, P.D., Thadani, V.M., Darcey, T.M., Mattson, R.H., Spencer, S.S., Spencer, D.D., 1993. Characteristics of medial temporal lobe epilepsy: I. Results of history and physical examination. Ann. Neurol. 34, 774–780.

Georgi, J.C., Stippich, C., Tronnier, V.M., Heiland, S., 2004. Active deep brain stimulation during MRI: a feasibility study. Magn. Reson. Med. 51, 380–388.

Goffin, K., Van, P.W., Van, L.K., 2011. In vivo activation of endocannabinoid system in temporal lobe epilepsy with hippocampal sclerosis. Brain 134, 1033–1040.

Goldberg, E.M., Coulter, D.A., 2013. Mechanisms of epileptogenesis: a convergence on neural circuit dysfunction. Nat. Rev. Neurosci. 14, 337–349.

Gowers, W.R., 1881. Epilepsy and Other Chronic Convulsive Disorders: Their Causes, Symptoms and Treatment. J&A Churchill, London.

Ho, S.S., Berkovic, S.F., McKay, W.J., Kalnins, R.M., Bladin, P.F., 1996. Temporal lobe epilepsy subtypes: differential patterns of cerebral perfusion on ictal SPECT. Epilepsia 37, 788–795.

Jones, S.E., Zhang, M., Avitsian, R., Bhattacharyya, P., Bulacio, J., Cendes, F., Enatsu, R., Lowe, M., Najm, I., Nair, D., Phillips, M., Gonzalez-Martinez, J., 2014. Functional magnetic resonance imaging networks induced by intracranial stimulation may help defining the epileptogenic zone. Brain Connect. 4, 286–298.

Kolster, H., Mandeville, J.B., Arsenault, J.T., Ekstrom, L.B., Wald, L.L., Vanduffel, W., 2009. Visual field map clusters in macaque extrastriate visual cortex. J. Neurosci. 29, 7031–7039.

Laufs, H., Rodionov, R., Thornton, R., Duncan, J.S., Lemieux, L., Tagliazucchi, E., 2014. Altered fMRI connectivity dynamics in temporal lobe epilepsy might explain seizure semiology. Front. Neurol. 5.

Logothetis, N.K., Augath, M., Murayama, Y., Rauch, A., Sultan, F., Goense, J., Oeltermann, A., Merkle, H., 2010. The effects of electrical microstimulation on cortical signal propagation. Nat. Neurosci. 13, 1283–1291.

Mathern, G.W., Babb, T.L., Vickrey, B.G., Melendez, M., Pretorius, J.K., 1995. The clinical-pathogenic mechanisms of hippocampal neuron loss and surgical outcomes in temporal lobe epilepsy. Brain 118 (Pt 1), 105–118.

McLaren, D.G., Kosmatka, K.J., Oakes, T.R., Kroenke, C.D., Kohama, S.G., Matochik, J.A., Ingram, D.K., Johnson, S.C., 2009. A population-average MRI-based atlas collection of the rhesus macaque. NeuroImage 45, 52–59.

Messinger, A., Seidlitz, J.M., Tootell, R.B., Underleider, L.G., 2014. Projections of the lateral and basal nuclei of the monkey amygdala delineated with electrical stimulation and fMRI. Program No.823.05. Soc. Neurosci. Abstr.

Moeller, S., Freiwald, W.A., Tsao, D.Y., 2008. Patches with links: a unified system for processing faces in the macaque temporal lobe. Science 320, 1355–1359.

Nelissen, N., Van Paesschen, W., Baete, K., Van Laere, K., Palmini, A., Van Billoen, H., Dupont, P., 2006. Correlations of interictal FDG-PET metabolism and ictal SPECT perfusion changes in human temporal lobe epilepsy with hippocampal sclerosis. NeuroImage 32, 684–695.

O'Brien, T.J., O'Connor, M.K., Mullan, B.P., Brinkmann, B.H., Hanson, D., Jack, C.R., So, E.L., 1998. Subtraction ictal SPET co-registered to MRI in partial epilepsy: description and technical validation of the method with phantom and patient studies. Nucl. Med. Commun. 19, 31–45.

Pittau, F., Grova, C., Moeller, F., Dubeau, F., Gotman, J., 2012. Patterns of altered functional connectivity in mesial temporal lobe epilepsy. Epilepsia 53, 1013–1023.

Premereur, E., Van Dromme, I.C., Romero, M.C., Vanduffel, W., Janssen, P., 2015. Effective connectivity of depth-structure-selective patches in the lateral bank of the macaque intraparietal sulcus. PLoS Biol. 13, e1002072.

Saleem, K.S., Logothetis, N.K., 2007. A Combined MRI and Histology Atlas of the Rhesus Monkey Brain in Stereotaxic Coordinates. Academic Press.

Spencer, S.S., 2002. Neural networks in human epilepsy: evidence of and implications for treatment. Epilepsia 43, 219–227.

Stefurak, T., Mikulis, D., Mayberg, H., Lang, A.E., Hevenor, S., Pahapill, P., Saint-Cyr, J., Lozano, A., 2003. Deep brain stimulation for Parkinson's disease dissociates mood and motor circuits: a functional MRI case study. Mov. Disord. 18, 1508–1516.

Styner, M., Knickmeyer, R., Joshi, S., Coe, C., Short, S.J., Gilmore, J., 2007. Automatic Brain Segmentation in Rhesus Monkeys. Proc. of SPIE 6512.

Sutula, T.S., Ockuly, J., 2006. In: Pitkanen, A., Schwartzkroin, P.A., Moshé, S.L. (Eds.), Kindling, spontaneous seizures, and the consequences of epilepsy: more than a model. Elsevier Academic Press, Models of Seizures and Epilepsy, pp. 395–406.

Tolias, A.S., Sultan, F., Augath, M., Oeltermann, A., Tehovnik, E.J., Schiller, P.H., Logothetis, N.K., 2005. Mapping cortical activity elicited with electrical microstimulation using FMRI in the macaque. Neuron 48, 901–911.

Tousseyn, S., Dupont, P., Goffin, K., Sunaert, S., Van Paesschen, W., 2015. Correspondence between large-scale ictal and interictal epileptic networks revealed by single photon emission computed tomography (SPECT) and electroencephalography (EEG)-functional magnetic resonance imaging (fMRI). Epilepsia 56, 382–392.

van Mierlo, P., Papadopoulou, M., Carrette, E., Boon, P., Vandenberghe, S., Vonck, K., Marinazzo, D., 2014. Functional brain connectivity from EEG in epilepsy: seizure prediction and epileptogenic focus localization. Prog. Neurobiol. 121, 19–35.

Van Paesschen, W., Dupont, P., Van Driel, G., Van Billoen, H., Maes, A., 2003. SPECT perfusion changes during complex partial seizures in patients with hippocampal sclerosis. Brain 126, 1103–1111.

Van Paesschen, W., Dupont, P., Sunaert, S., Goffin, K., Van Laere, K., 2007. The use of SPECT and PET in routine clinical practice in epilepsy. Curr. Opin. Neurol. 20, 194–202.

Vanduffel, W., Fize, D., Mandeville, J.B., Nelissen, K., Van Hecke, P., Rosen, B.R., Tootell, R.B., Orban, G.A., 2001. Visual motion processing investigated using contrast agent-enhanced fMRI in awake behaving monkeys. Neuron 32, 565–577.

Wada, J.A., Mizoguchi, T., Osawa, T., 1978. Secondarily generalized convulsive seizures induced by daily amygdaloid stimulation in rhesus monkeys. Neurology 28, 1026–1036.

Walovitch, R.C., Hill, T.C., Garrity, S.T., Cheesman, E.H., Burgess, B.A., O'Leary, D.H., Watson, A.D., Ganey, M.V., Morgan, R.A., Williams, S.J., 1989. Characterization of technetium-99m-L,L-ECD for brain perfusion imaging, Part 1: Pharmacology of technetium-99m ECD in nonhuman primates. J. Nucl. Med. 30, 1892–1901.

Yaffe, R.B., Borger, P., Megevand, P., Groppe, D.M., Kramer, M.A., Chu, C.J., Santaniello, S., Meisel, C., Mehta, A.D., Sarma, S.V., 2015. Physiology of functional and effective networks in epilepsy. Clin. Neuropathol. 126, 227–236.